Nano Energy xxx (xxxx) xxx

Contents lists available at ScienceDirect

Nano Energy

journal homepage: http://www.elsevier.com/locate/nanoen

Full paper

A linear-to-rotary hybrid nanogenerator for high-performance wearable biomechanical energy harvesting

Cheng Yan [a,1], Yuyu Gao [a,1], Shenlong Zhao [b], Songlin Zhang [b], Yihao Zhou [b], Weili Deng [a,**], Ziwei Li [a], Gang Jiang [a], Long Jin [a], Guo Tian [a], Tao Yang [a], Xiang Chu [a], Da Xiong [a], Zixing Wang [a], Yongzhong Li [b], Weiqing Yang [a,***], Jun Chen [b,*]

[a] Key Laboratory of Advanced Technologies of Materials (Ministry of Education), School of Materials Science and Engineering, Southwest Jiaotong University, Chengdu 610031, PR China

[b] Department of Bioengineering, University of California, Los Angeles, Los Angeles, CA 90095, USA

ARTICLE INFO

Keywords:
Biomechanical energy
Nanogenerator
Wearable electronics
Body area network
Personalized health care

ABSTRACT

Harvesting biomechanical energy from low-frequency human body motions is a challenging but promising approach to powering the future wearables. Herein, we report a linear-to-rotary hybrid nanogenerator (LRH-NG) to effectively harvest low-frequency body biomechanical energy via a frequency enhancement strategy. Remarkably, the generated current and voltage by the LRH-NG from human body movement are respectively enhanced up to 3.1 times and 3.6 times of that at the basic frequency (2 Hz). Furthermore, the LRH-NG was demonstrated as an on-body electricity generator that can sustainably power a body area network with a temperature sensor and a humidity sensor for personalized health care. The designed LRH-NG may open up a new approach for high-performance low-frequency wearable biomechanical energy harvesting as a sustainable and pervasive energy solution in the era of the Internet of things.

1. Introduction

Efficient energy harvesting devices are attracting intensive research endeavors, aiming at providing a sustainable and pervasive energy solution for the on-body electronics, personalized health care and artificial intelligence in the foreseeable future [1–10]. In comparison to traditional power supply units such as batteries, on-body mechanical energy harvesters have characteristics of being sustainable and renewable [11,12], and have been increasingly considered as the ideal energy solution for distributed electronics in the era of Internet of things [13–15]. In the past decades, various energy technologies based on piezoelectric [3,7,16,17], electromagnetic [18] and triboelectric effects [19–25] have been brilliantly pullulated for converting ambient mechanical energy into electricity, among which electromagnetic generators (EMGs) based on Faraday's law of electromagnetic induction and triboelectric nanogenerators (TENGs) derived from Maxwell's displacement current [26–28] are considered as the two most effective approaches. On one hand, the majority of mechanical motions from the human body is in the low-frequency range (less than 10 Hz), which renders a challenge to both EMGs and TENGs [29,30]. Furthermore, biomechanical movements associated with the human body is usually linear, such as the vibration from human walking and running [31]. Wide working bandwidth is the predominant factor for efficient vibration energy harvesting, and is a challenging problem needed to be addressed in the community [12,32–34]. On the other hand, both TENGs and EMGs are superior solutions to generate electricity from rotary motions due to their intrinsic working principles [35–40].

In this regard, we report a linear-to-rotary hybrid nanogenerator (LRH-NG) as an effective approach to generate electricity from low-frequency human biomechanical movement as a sustainable power source to drive a body area network for personalized healthcare. With a rational design, the LRH-NG could first convert on-body linear biomechanical motion into rotational motion and efficiently generate electricity to power a temperature sensor and a humidity sensor for

* Corresponding author.
** Corresponding author.
*** Corresponding author.
E-mail addresses: weili1812@swjtu.edu.cn (W. Deng), wqyang@swjtu.edu.cn (W. Yang), jun.chen@ucla.edu (J. Chen).
[1] These authors contributed equally to this work.

https://doi.org/10.1016/j.nanoen.2019.104235
Received 9 September 2019; Received in revised form 13 October 2019; Accepted 24 October 2019
Available online 1 November 2019

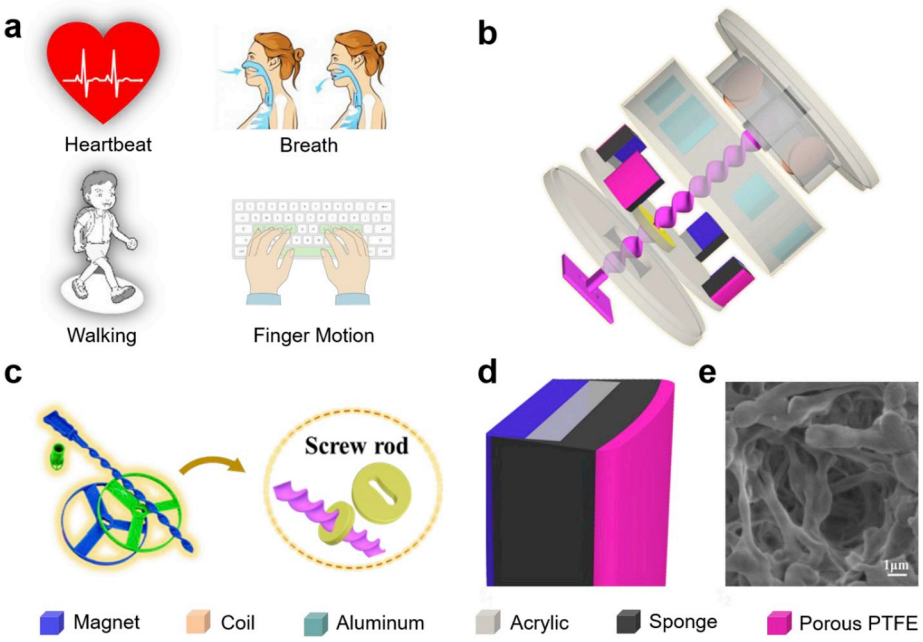

Fig. 1. Structural design of linear-to-rotary hybrid nanogenerator (LRH-NG). (a) The majority of biomechancial motions accosiated with human body, such as heartbeat, breath, walking, and finger motion, are in the low-frequency range. (b) Schematic illustration of the proposed LRH-NG. (c) An illurstation showing the disc with a peanut-shape hole, a threaded rod, and the procedure of converting linear motions into rotary motions. (d) An enlarged view of the square pillar showing its multilayered structure. (e) A SEM image of the porous PTFE as a triboelectric layer.

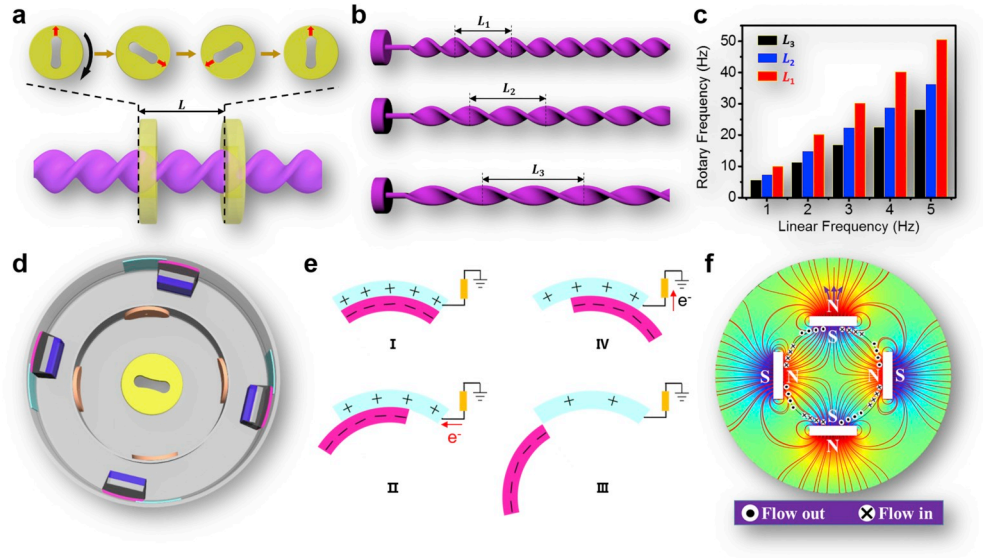

Fig. 2. Operating principle of the LRH-NG. (a) An illustration of the discs with peanut-shaped holes (top) and a threaded rod (bottom). *L* denotes the periodic length. When the disc moves linearly along the threaded rod, the disc starts spinning and converts the linear biomechanical motions into rotatory mechanical motions. (b) A illustration showing the threaded rod with different periodic lengths. (c) The dependence of the frequency enhancement factor on the periodic length of the threaded rod. (d) A three-dimensional top-view of the electricity generation part of the LRH-NG. (e) A cycle of the electricity generation processing from (e) the TENG component, and (f) the EMG component.

continuous biomonitoring. The LRH-NG paves a new way to efficiently utilize the low-frequency body biomechanical motion for on-body electronics in the era of Internet of things with a wide-range of applications.

2. Results and discussion

The majority of biomechanical energy from body motions are in the low-frequency range, as illustrated in Fig. 1a. To effectively harness low-frequency biomechanical motions, a novel linear-to-rotary hybrid nanogenerator (LRH-NG) was developed, as schematically depicted in Fig. 1b. The LRH-NG mainly consists of three parts including a threaded rod, a rotator and a stator, as illustrated in Fig. 1c (see Supporting Note 1 for the detailed idea). The rotator was composed of four-square pillars and each had a four-layer structure. From the inmost to outmost, they are bar magnet, acrylic, soft sponge, and porous polytetrafluoroethylene (PTFE). The bar magnets were fixed on the acrylic substrate. A layer of soft sponge next to the acrylic is the buffering layer to enhance both the triboelectrification and device robustness. On top of the sponge, a layer of porous PTFE was laminated as one of the triboelectric layers. An enlarged view of the rotator of the LRH-NG is shown in Fig. 1d. In the stator, four groups of coils were evenly anchored onto the inner wall, which will pair up with magnets to form four sets of EMGs. Four pieces of aluminum foil were also employed as both the electrodes and another triboelectric layers, pairing with the PTFE to form the four sets of TENGs. As a consequence, the rational design of the LRH-NG could effectively convert the threaded rod linear motion into the rotationally sliding motion of the rotator. More details of the fabrication procedures of the LRH-NG are presented in both the Experimental Section and Fig. S1.

The working principle of the LRH-NG for energy harvesting could be explained from both mechanical and electrical perspectives. Fig. 2a shows the illustration of the discs with peanut-shaped holes (top) and a threaded rod (bottom). *L* denotes the periodic length. Mechanically,

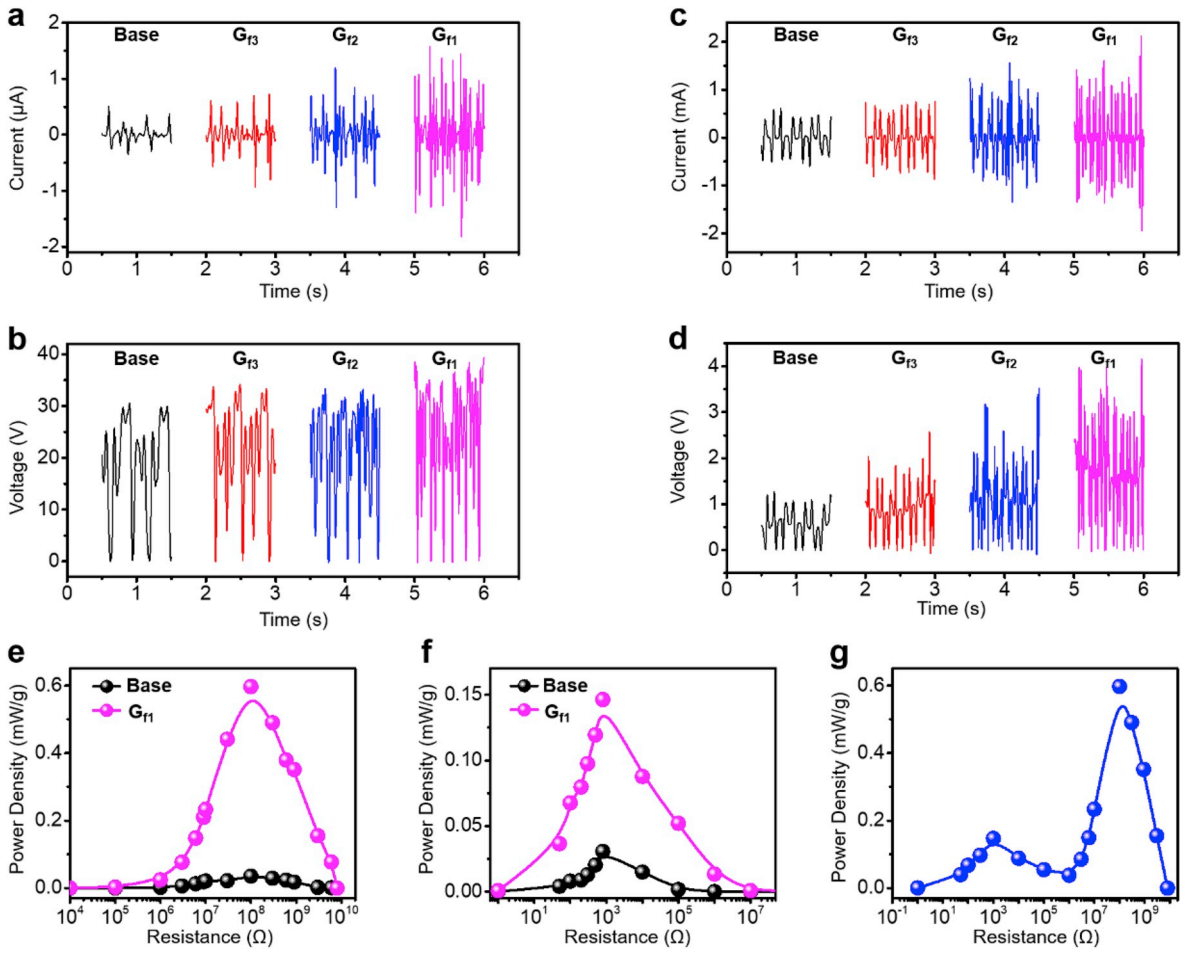

Fig. 3. Electrical output performance of the LRH-NG. Comparison of (a) the current and (b) voltage output of the TENG, (c) the current and (d) voltage output of the EMG at both basic and enhanced frequencies under a same bioemechanical input. Dependence of the peak power density on the loading resistances of the (e) TENG and (f) EMG at base frequency and with the frequency enhancement factor G_{f1}. (g) Dependence of the output current and power density of the LRH-NG on the external loading resistances.

when the disc with the peanut-shaped hole moves linearly along the threaded rod, the disc starts spinning and convert the linear biomechanical motions into rotatory mechanical motions. Here, the periodic length plays an important role of determining the rotation speed of the disc. Fig. 2b shows the threaded rod with different periodic lengths. The shorter the periodic length, the higher the rotation speed reached at a given linear motion speed, as shown in Fig. 2c. Theoretically, the frequency enhancement factor G_f can be calculated according to the following equation:

$$G_f = \frac{2\pi D}{L} \tag{1}$$

where D is the radius of disc, and L is the periodic length of the threaded rod, as illustrated in Fig. S2. From equation (1), it can be seen that the frequency enhancement factor G_f is directly proportional to the disc radius, inversely proportional to the periodic length of the threaded rod. The electricity generation from biomechanical motions can be elucidated from two pathways: TENG and EMG. For a better interpretation, a three-dimensional top-view of the electricity generation part of the LRH-NG is exhibited in Fig. 2d. A cycle of electricity generation from the triboelectric nanogenerator is presented in Fig. 2e. At the original stage I, when the porous PTFE film was driven to contact with aluminum (Al) foil, electrons would transfer from the Al electrode to the porous PTFE, with the PTFE becoming negatively charged while the aluminum becomes positively charged due to their electron affinity difference (Table S1). These static charges are non-mobile and will sustain on the surfaces for a long period of time. When disc starts spinning, a relative displacement was induced between PTFE and Al coil, which drives the free electrons to flow from the ground to the aluminum (stage II). With further spinning, the flow of induced electrons continues until a new electrical equilibrium is established (stage III). A continuous rotational motion will lead to a reverse flow of electrons (stage IV). The electricity generation from the electromagnetic generator component can be verified via COMSOL, as the simulation result shows in Fig. 2f. The biomechanical motion induced magnetic flux change in the coils will generate electricity. A full cycle of the electricity generation processing of the EMG is presented in Fig. S3. The LRH-NG could convert low-frequency linear biomechanical motions into high-frequency electrical signals.

To systematically investigate the peak power output of the as-fabricated LRH-NG for effectively harvesting low frequency biomechanical energy, a programming controlled linear motor was employed to drive the LRH-NG, as the measurement setup revealed in Fig. S4a. Fig. S4b shows the digital photos of the 3D printed threaded rods with three different periodic lengths, corresponding to three different frequency enhancement factors (G_{f1}, G_{f2} and G_{f3}). To quantify the frequency enhancement, we set a basic frequency of 2 Hz (see Supporting Note 2 for details). As indicated in Fig. 3a, the current output of the LRH-NG was significantly improved. Specifically, the peak current value observed at G_{f1} is 3.1 times higher than that obtained at basic frequency without frequency enhancement, while the voltage amplitude keeps constant, as demonstrated in Fig. 3b. Furthermore, the output

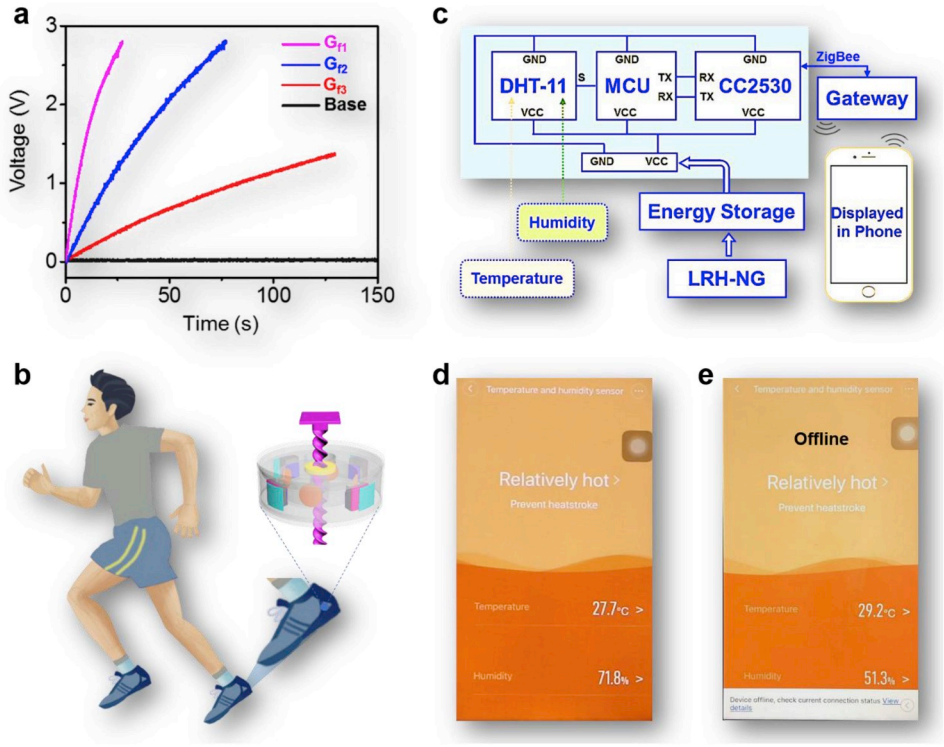

Fig. 4. Demonstration of the LRH-NG as a sustainable power source to drive a body area network for personalized health care. (a) The charging curves of a commercial capacitor (220 μF) by LRH-NGs with different frequency enhancement factors. (b) An illustration showing a LRH-NG for energy harvesting from human walking. (c) The system configuration of the LRH-NG as the integrated power-supplying component of a body area network for personalized health care. (d) The energy generated from human walking by the LRH-NG with an enhancement factor of G_{f1} could power a body area network for continous biomonitering. The temperature and humidity information around human body could be measured and simultaneously displayed on a cellphone. (e) Under the same conditions, the energy generated by the hybridized nanogenerator without frequency enhancement was incapable of powering the body area network.

performance of a linear-to-rotary EMG unit was also evaluated with the same frequency enhancement factor, as the results show in Fig. 3c. And the output current was increased by about 3.4 times, 2.6 times and 1.5 times in comparison to that at basic frequency for the LR-EMGs with G_{f1}, G_{f2} and G_{f3}, respectively. Fig. 3d shows that the voltage is increased by about 3.6 times, 2.8 times and 1.8 times, respectively. It is worth noting that, the frequency enhancement factor can not only increase the amplitudes, but also the peak density of both current and voltage signals, resulting in a greatly improved output power.

To evaluate the output peak power of the LRH-NG, external resistors were utilized as the load resistances. As displayed in Fig. 3e, the instantaneous peak power density ($I^2_{peak}R$) for both basic frequency and G_{f1} were maximized at a load resistance of 10^8 Ω. Moreover, the peak power dramatically increases for LR-TENG when employing a threaded rod, reaching up to 0.59 mW/g with G_{f1}, almost 16 times higher than that at basic frequency. Similar trends for G_{f2} and G_{f3} were found in Fig. S5a that the peak power density was enhanced 9 times and 4 times, respectively. For a single LR-EMG unit as shown in Fig. 3f, with a load resistance of 10^3 Ω, the peak power density reached a maximum value (0.146 mW/g) under the frequency enhancement factor G_{f1}, which is 4.7 times higher than that at the basic frequency. The dependence of the peak power density on the load resistances of EMG with G_{f2} and G_{f3} further demonstrated an enhancement of 3.1 times and 1.9 times, respectively, as plotted in Fig. S5b. After the optimization of the output performance of individual TENG and EMG components, overcoming the impedance mismatch between the two needs to be addressed for high-performance biomechanical energy harvesting. As plotted in Fig. 3g, the instantaneous peak power density of the LRH-NG by integrating one TENG unit and one EMG unit under the frequency condition of G_{f1} shows a wide range of load resistances from 10^3 Ω to 10^8 Ω. In addition, the device robustness is also very important towards practical energy harvesting. As elaborated in Fig. S6, with the systematic integration of four pairs of TENG and EMG units, the hybrid nanogenerator can produce a current up to 8 mA with a rectifier and the current amplitudes showed negligible changes after more than 4000 cycles of operation.

To demonstrate the LRH-NG as a sustainable power source, a commercial capacitor (220 μF) was charged by the LRH-NG at basic frequency and three different enhancement frequency (G_{f1}, G_{f2}, and G_{f3}), as shown in Fig. 4a. The LRH-NG with smaller periodic length (corresponding to the larger frequency enhancement factor) brought about a highest charging rate. Moreover, the LRH-NG can be embedded in shoes to harvest the low-frequency biomechanical energy from human walking. As a proof-of-concept demonstration, the LRH-NG powered a body area network as shown in Fig. 4b. The small body area network consists of a wireless temperature sensor and a humidity sensor (Fig. S7). The LRH-NG was demonstrated as an integrated sustainable power-supplying system to drive the sensor network for personalized health care. Fig. 4c is the system configuration of the self-powered body area network. As shown in Fig. S8, the LRH-NG at G_{f1} can charge a commercial capacitor of 1 mF in the system of temperature and humidity sensors from 0 V to 3.1 V in about 83 s. The inset represented an enlarged view of the charging processing and the green part demonstrated a whole cycle of charging and discharging process. The ambient temperature and humidity information around human body measured by the sensors was displayed on a cellphone (Fig. 4d). As shown in supporting Video S1, in the indoor environment, the temperature of 26.5 °C and humidity of 70.9% were displayed on the cellphone (Fig. S9a). After an expiration, both temperature and humidity increased to 30.2 °C and 97.9% (Fig. S9b), respectively. A reminder showing "prevent heatstroke and start dehumidification" enables the possibility of personalized health care. Finally, the environment turns to "Damp" when the person entered an environment with cold wind blowing (Fig. S9c). To compare, the hybridized nanogenerator without frequency enhancement was also applied to power the same body area network during normal human walking. However, the display status in the cellphone indicated "Device Offline" , as shown at the bottom of the screen (Fig. 4e).

Supplementary video related to this article can be found at https://doi.org/10.1016/j.nanoen.2019.104235.

3. Conclusion

In summary, we presented a linear-to-rotary hybrid nanogenerator for low-frequency human body biomechanical energy harvesting. The reported LRH-NG was demonstrated as an integrated and sustainable power-supplying system to a body area network for personalized health care. It was demonstrated to drive a wireless temperature and humidity sensing system for continuous biomonitoring. This newly designed LRH-NG not only provides a novel approach for wearable biomechanical energy harvesting as a pervasive energy solution for the distributed electronics, but also can be extended to improve the energy harvesting from other low-frequency mechanical motions in nature, including engine vibration, bridge vibration, ocean waves, and so on.

4. Experimental Section

Fabrication of the linear-to-rotary hybrid nanogenerator: The framework of the device was constructed with two acrylic tubes and two acrylic sheets. First, the supporting substrates were processed by a laser cutter (TR-6040). Four groups of coils were evenly attached onto the inner wall of the acrylic tube with a diameter of 80 mm. Second, four square pillars were uniformly and symmetrically fixed around the disc with a peanut-shape hole and physical gap in between. Each of the square pillar was stacked with layers of magnet, acrylic, sponge and porous PTFE film. Four aluminum foils with dimensions of 30 mm × 20 mm were attached to the inner wall of acrylic tube with a diameter of 95 mm.

***Materials Characterization and Device Measurements*:** The microstructure on the surface of the porous PTFE was characterized by the scanning electron microcopy (SEM) (JEOL JSM-7001F). The output voltage was measured by a low-noise voltage preamplifier (Keithley-6514 system electrometer). The output current of the device was measured by a low-noise current preamplifier (Stanford Research SR570).

Declaration of competing interest

The authors declare no competing financial interest.

Acknowledgments

J. C., W. Y. and W.D. supervised and guided the whole project. C. Y. and Y. G. contributed equally to this work. J.C. submitted the manuscript and was the lead contact. This research was financially supported by the National Natural Science Foundation of China (No. 61801403), the Independent Research Project of State Key Laboratory of Traction Power (No. 2017TPL_Z04), Miaozi Project of Sichuan province, and the Fundamental Research Funds for the Central Universities of China (No. 2682017CX071). The authors gratefully acknowledge the Analysis and Testing Center of Southwest Jiaotong University. The authors also gratefully acknowledge ceshigo (www.ceshigo.com) for providing testing services. J.C., S. Z., and Y. Z. acknowledge the Henry Samueli School of Engineering & Applied Science and the Department of Bioengineering at the University of California, Los Angeles for the startup support.

Appendix A. Supplementary data

Supplementary data to this article can be found online at https://doi.org/10.1016/j.nanoen.2019.104235.

References

[1] Z.L. Wang, Nano Energy 58 (2019) 669–672.
[2] Z.L. Wang, Nano Energy 54 (2018) 477–483.
[3] Z.L. Wang, J. Song, Science 312 (2006) 242–246.
[4] Y. Yang, W. Gao, Chem. Soc. Rev. 48 (2019) 1465–1491.
[5] S. Wang, J. Xu, W. Wang, G.N. Wang, R. Rastak, F. Molina-Lopez, J.W. Chung, S. Niu, V.R. Feig, J. Lopez, T. Lei, S.K. Kwon, Y. Kim, A.M. Foudeh, A. Ehrlich, A. Gasperini, Y. Yun, B. Murmann, J.B. Tok, Z. Bao, Nature 555 (2018) 83–88.
[6] C. Wang, X. Li, H. Hu, L. Zhang, Z. Huang, M. Lin, Z. Zhang, Z. Yin, B. Huang, H. Gong, S. Bhaskaran, Y. Gu, M. Makihata, Y. Guo, Y. Lei, Y. Chen, C. Wang, Y. Li, T. Zhang, Z. Chen, A.P. Pisano, L. Zhang, Q. Zhou, S. Xu, Nat. Biomed. Eng. 2 (2018) 687–695.
[7] C. Yan, W. Deng, L. Jin, T. Yang, Z. Wang, X. Chu, H. Su, J. Chen, W. Yang, ACS Appl. Mater. Interfaces 10 (2018) 41070–41075.
[8] J. Shintake, V. Cacucciolo, D. Floreano, H. Shea, Adv. Mater. 30 (2018) 1707035.
[9] Y. Kim, A. Chortos, W. Xu, Y. Liu, J.Y. Oh, D. Son, J. Kang, A.M. Foudeh, C. Zhu, Y. Lee, S. Niu, J. Liu, R. Pfattner, Z. Bao, T.-W. Lee, Science 360 (2018) 998–1003.
[10] B. Chu, W. Burnett, J.W. Chung, Z. Bao, Nature 549 (2017) 328–330.
[11] W. Yang, J. Chen, G. Zhu, J. Yang, P. Bai, Y. Su, Q. Jing, X. Cao, Z.L. Wang, ACS Nano 7 (2013) 11317–11324.
[12] J. Chen, Z.L. Wang, Joule 1 (2017) 480–521.
[13] Z. Wen, M.-H. Yeh, H. Guo, J. Wang, Y. Zi, W. Xu, J. Deng, L. Zhu, X. Wang, C. Hu, L. Zhu, X. Sun, Z.L. Wang, Sci. Adv. 2 (2016) e1600097.
[14] R. Hinchet, S.-W. Kim, ACS Nano 9 (2015) 7742–7745.
[15] J. Wang, S. Li, F. Yi, Y. Zi, J. Lin, X. Wang, Y. Xu, Z.L. Wang, Nat. Commun. 7 (2016) 12744.
[16] W. Deng, T. Yang, L. Jin, C. Yan, H. Huang, X. Chu, Z. Wang, D. Xiong, G. Tian, Y. Gao, H. Zhang, W. Yang, Nano Energy 55 (2019) 516–525.
[17] G. Tian, W. Deng, Y. Gao, D. Xiong, C. Yan, X. He, T. Yang, L. Jin, X. Chu, H. Zhang, W. Yan, W. Yang, Nano Energy 59 (2019) 574–581.
[18] S. Zhou, C. Jean-Mistral, S. Chesné, Smart Mater. Struct. 27 (2018) 085015.
[19] J. Chen, Y. Huang, N. Zhang, H. Zou, R. Liu, C. Tao, X. Fan, Z.L. Wang, Nat. Energy 1 (2016) 16138.
[20] L. Zhang, B. Zhang, J. Chen, L. Jin, W. Deng, J. Tang, H. Zhang, H. Pan, M. Zhu, W. Yang, Z.L. Wang, Adv. Mater. 28 (2016) 1650–1656.
[21] G. Cheng, Z.-H. Lin, L. Lin, Z.-l. Du, Z.L. Wang, ACS Nano 7 (2013) 7383–7391.
[22] G. Cheng, H. Zheng, F. Yang, L. Zhao, M. Zheng, J. Yang, H. Qin, Z. Du, Z.L. Wang, Nano Energy 44 (2018) 208–216.
[23] H. Qin, G. Cheng, Y. Zi, G. Gu, B. Zhang, W. Shang, F. Yang, J. Yang, Z. Du, Z. L. Wang, Adv. Funct. Mater. 28 (2018) 1805216.
[24] J. Yang, F. Yang, L. Zhao, W. Shang, H. Qin, S. Wang, X. Jiang, G. Cheng, Z. Du, Nano Energy 46 (2018) 220–228.
[25] K. Zhao, G. Gu, Y. Zhang, B. Zhang, F. Yang, L. Zhao, M. Zheng, G. Cheng, Z. Du, Nano Energy 53 (2018) 898–905.
[26] Z.L. Wang, A.C. Wang, Mater. Today (2019), https://doi.org/10.1016/j.mattod.2019.05.016.
[27] D. Liu, X. Yin, H. Guo, L. Zhou, X. Li, C. Zhang, J. Wang, Z.L. Wang, Sci. Adv. 5 (2019) eaav6437.
[28] Z.L. Wang, Mater. Today 20 (2017) 74–82.
[29] Y. Zi, H. Guo, Z. Wen, M.H. Yeh, C. Hu, Z.L. Wang, ACS Nano 10 (2016) 4797–4805.
[30] C. Wu, R. Liu, J. Wang, Y. Zi, L. Lin, Z.L. Wang, Nano Energy 32 (2017) 287–293.
[31] I.-W. Tcho, S.-B. Jeon, S.-J. Park, W.-G. Kim, I.K. Jin, J.-K. Han, D. Kim, Y.-K. Choi, Nano Energy 50 (2018) 489–496.
[32] J. Yang, J. Chen, Y. Yang, H. Zhang, W. Yang, P. Bai, Y. Su, Z.L. Wang, Adv. Energy Mater. 4 (2014) 1301322.
[33] J. Chen, G. Zhu, W. Yang, Q. Jing, P. Bai, Y. Yang, T.C. Hou, Z.L. Wang, Adv. Mater. 25 (2013) 6094–6099.
[34] Y. Xie, S. Wang, S. Niu, L. Lin, Q. Jing, J. Yang, Z. Wu, Z.L. Wang, Adv. Mater. 26 (2014) 6599–6607.
[35] R. Cao, T. Zhou, B. Wang, Y. Yin, Z. Yuan, C. Li, Z.L. Wang, ACS Nano 11 (2017) 8370–8378.
[36] Y. Xie, S. Wang, L. Lin, Q. Jing, Z.-H. Lin, S. Niu, Z. Wu, Z.L. Wang, ACS Nano 7 (2013) 7119–7125.
[37] B. Zhang, J. Chen, L. Jin, W. Deng, L. Zhang, H. Zhang, M. Zhu, W. Yang, Z. L. Wang, ACS Nano 10 (2016) 6241–6247.
[38] C. Zhang, T. Zhou, W. Tang, C. Han, L. Zhang, Z.L. Wang, Adv. Energy Mater. 4 (2014) 1301798.
[39] Y. Xie, S. Wang, S. Niu, L. Lin, Q. Jing, Y. Su, Z. Wu, Z.L. Wang, Nano Energy 6 (2014) 129–136.
[40] D. Bhatia, J. Lee, H.J. Hwang, J.M. Baik, S. Kim, D. Choi, Adv. Energy Mater. 8 (2018) 1702667.